Gold Nanoparticles with Different Capping Systems: An Electronic and Structural XAS Analysis

C. López-Cartes,[†] T. C. Rojas,[†] R. Litrán,[†,‡] D. Martínez-Martínez,[†] J. M. de la Fuente,[§,||] S. Penadés,[||] and A. Fernández*[,†]

Instituto de Ciencia de Materiales de Sevilla, and Grupo Carbohidratos, Laboratory of Glyconanotechnology IIQ, CSIC−Universidad Sevilla, Américo Vespucio nr. 49, 41092-Sevilla, Spain

Received: January 11, 2005; In Final Form: March 3, 2005

Gold nanoparticles (NPs) have been prepared with three different capping systems: a tetralkylammonium salt, an alkanethiol, and a thiol-derivatized neoglycoconjugate. Also gold NPs supported on a porous TiO_2 substrate have been investigated. X-ray absorption spectroscopy (XAS) has been used to determine the electronic behavior of the different capped/supported systems regarding the electron/hole density of d states. Surface and size effects, as well as the role of the microstructure, have been also studied through an exhaustive analysis of the EXAFS (extended X-ray absorption fine structure) data. Very small gold NPs functionalized with thiol-derivatized molecules show an increase in d-hole density at the gold site due to Au−S charge transfer. This effect is overcoming size effects (which lead to a slightly increase of the d-electron density) for high S:Au atomic ratios and core−shell microstructures where an atomically abrupt Au−S interface likely does not exist. It has been also shown that thiol functionalization of very small gold NPs is introducing a strong distortion as compared to fcc order. To the contrary, electron transfer from reduced support oxides to gold NPs can produce a higher increase in d-electron density at the gold site, as compared to naked gold clusters.

Introduction

Nanostructured materials are characterized by the existence of particles/phases in the 1−10 nm range, where size reduction effects may originate either unusual or different properties from corresponding bulk materials.[1] On the other hand, the high surface-to-bulk ratio of these materials produces also important effects due to surface anisotropy or surface functionalization.[2] In particular, the "nanosize effect" in small gold particles may result in stronger d−d interaction so that the d electron charge will increase at the Au site relative to the bulk.[2−4] Further, when the size of the nanoparticles decreases, a larger fraction of metal atoms will be located on the surface. As a result, the optimization of surface energy (reduced coordination number) and the metal−substrate or metal−adsorbate[5,6] interactions will influence the electronic structure of the transition metal. It has been shown that one can modify the electronic behavior of gold nanoparticles by carefully controlling their surface environments. In a previous paper,[4] Zhang and Sham have reported that the d electron (or hole) distribution of ∼2 nm Au nanoparticles (NPs) can be tuned by selective capping, that is, the NPs gain d electrons when capped with a weakly interacting dendrimer molecule but lose d electrons when capped with the strongly interacting thiols. The electronic behavior of the capped Au NPs were monitored in these previous papers by X-ray absorption near-edge structure (XANES), a technique that is very sensitive to the d-charge redistribution of transition metals induced by a change of local environments.[7,8] Very recently,[9] we also showed that the tuning of the electronic structure and total number of d holes in Au NPs, by controlling different capping and size, also tunes the magnetic properties of the nanoparticles.

In the present paper, we combine the XANES with the EXAFS analysis for gold nanoparticles stabilized with different capping systems (including functionalization, surface modification, or protection by dipole interactions). Thiol-stabilized nanoparticles with diameter smaller than 2 nm, changing also the nature of the functionalizing molecule, have been analyzed in comparison to alkylammonium-stabilized nanoparticles and to gold nanoparticles supported on titania substrates. The structural information obtained by EXAFS analysis, combined with the electronic information obtained by XANES, allows us to distinguish size effects producing contraction of the gold lattice from surface modification effects associated with the different environments. Of special interest are the results presented here regarding the formation of a modified Au−S shell in very small thiol-functionalized Au NPs together with the introduction of disordered in the gold clusters showing no abrupt Au−S interfaces. The relevance of these results for understanding the singular new magnetic and electronic behavior[9] of Au NPs should be emphasized.

Experimental Section

Gold nanoparticles stabilized with different capping systems have been prepared by the chemical reduction of a metal salt precursor (hydrogen tetrachloroaurate, $HAuCl_4$) in a liquid phase, in the presence of "protective" species that, due to the formation of covalent links or by electrostatic interactions,

* Corresponding author. Telephone: +34 954489531. Fax: +34 954450665. E-mail: asuncion@icmse.csic.es.
[†] Instituto de Ciencia de Materiales de Sevilla.
[‡] Present address: Departamento de Física de la Materia Condensada, Universidad de Cádiz.
[§] Present address: Departamento Centre for Cell Engineering, Institute of Biomedical and Life Science, Joseph Black Building, University of Glasgow, Glasgow, G12 8QQ, UK.
[||] Grupo Carbohidratos, Laboratory of Glyconanotechnology IIQ.

10.1021/jp050184+ CCC: $30.25
Published on Web 04/05/2005

SCHEME 1: Schematic Structures of Capped Gold NPs

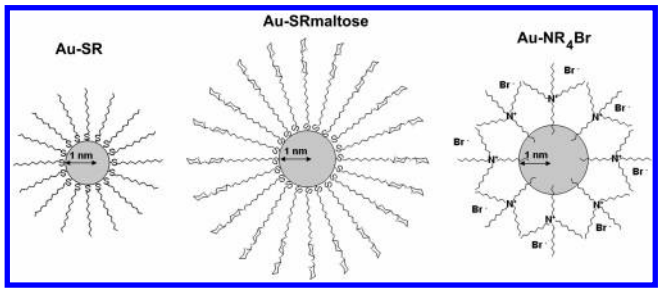

TABLE 1: Description, Size, and Composition Data for the Different Gold NPs under Investigation

sample	S/Au (EDX)[a]	N + C/Au (EDX)[a]	metal loading (wt %)[b]	D^c (nm)	total Nr[d]	% Nr[d]
AuSR	1.00			1.4	55	76
Au−SRmaltose	0.60			1.8	147	63
Au−NR_4Br		0.83		1.5−5		
Au−$TiO_2(Ti^{3+})$			4	2	180	59

[a] Semiquantitative atomic ratios as measured by EDX. [b] Percentage by weight of supported metal. [c] Average particle size as calculated from particle size distribution histograms. Sample Au−NR_4Br shows a bimodal distribution centered at 1.5 and 5 nm (see Figure 1c). [d] Total Nr: calculated number of atoms for a pure gold cluster. %Nr: calculated percentage of atoms located at the surface of a pure gold cluster.

isolate the metal cluster, preventing its growth. Scheme 1 represents the different capped Au NPs under investigation.

The Au−SR sample (Scheme 1), constituted by dodecanethiol-derivatized gold NPs, was prepared by the Brust method.[10] In this case a thiol:gold ratio of 2.0 was used in the starting solutions in order to decrease the particle size average.[11] For the preparation of the Au−SRmaltose sample (Scheme 1), a malto-neoglycoconjugate was used as thiol linker species. The preparation of these thiol-derivatized gold glyconanoparticles was done by a modification of the Brust method and has been extensively described in ref 12. In both cases, preparation was done at room temperature with natural heating produced upon reduction reaction.

With the aim to compare the influence of the protective species on the electronic and structural behavior of the gold metal clusters, tetraalkylammonium-protected gold NPs have also been prepared. This one-step redox-controlled size method consisted of the chemical reduction of the precursor salt using sodium borohydride as reducing agent in the presence of a stabilizer of the type $R_4N^+X^-$ (tetraoctylammonium bromide in this case). The so-called Au−NR_4Br nanoparticles have been obtained (Scheme 1).

In addition to the capped NPs described above, we did also study gold nanoparticles supported on colloidal titania. This sample was obtained by the photocatalytic reduction of gold on a colloidal TiO_2 sample[13] and will be named hereafter the Au−$TiO_2(Ti^{3+})$ sample.

Table 1 summarizes the description, size, and composition data for the different gold NPs under investigation.

TEM analysis was carried out with a Philips CM200 microscope working at 200 kV with a LaB_6 filament. Particle size distribution histograms were measured using an automatic image analyzer.

X-ray absorption spectra (XAS) for capped Au NPs were recorded at room temperature in transmission mode at the beam line BM29 in the ESRF storage ring in samples supported on cellulose filters. Spectra were recorded at the Au L_{III} edge at 11 920 eV. To compare the XANES region of the XAS spectra,

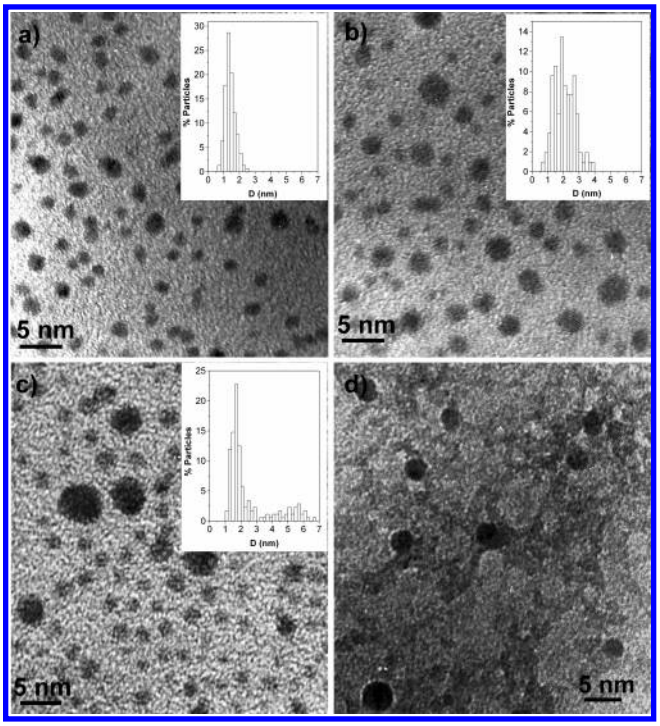

Figure 1. Transmission electron micrographs of Au−SR (a), Au−SRmaltose (b), Au−NR_4Br (c), and Au−$TiO_2(Ti^{3+})$ (d) NPs. The corresponding particle size distribution histograms of the capped nanoparticles are also included.

a linear background was fitted in the pre-edge region and subtracted before normalization to the edge jump. Qualitative interpretation of the EXAFS oscillations was done based on FEFF6 real space single scattering calculations for suitable cluster models.[14] The cluster models were generated by using RHODIUS program.[15] The EXAFS oscillations were quantitatively analyzed with the software package developed by Bonin et al.[16] The coordination numbers (N), distances (R), and Debye−Waller factors (σ) were extracted by a least-squares fitting procedure that uses the theoretical phases and amplitudes proposed by Rehr and co-workers[14] previously calibrated with the appropriate reference (Au foil).

XANES spectra at the Au L_{III} edge for the Au−$TiO_2(Ti^{3+})$ sample were recorded at the XAS3 line in the LURE Synchrotron as described in ref 13.

Results and Discussion

Figure 1 shows the TEM micrographs for the capped gold NPs. Several micrographs were used to elaborate particle size distribution histograms for the three samples (see Figure 1a−c), and the calculated average particles sizes are shown in Table 1. Gold NPs present, in all the cases, narrow particle size distribution, except for sample Au−NR_4Br, where a bimodal distribution was observed centered at 1.5 and 5.0 nm. The different microstructures of the capped (Au−SR, Au−SRmaltose, and Au−NR_4Br) and the supported (Au−$TiO_2(Ti^{3+})$) nanoparticles are also shown in Figure 1. In the last sample (Figure 1d) we also observe, with a lighter contrast, the porous titania phase supporting the gold NPs.

Figure 2 shows the XANES spectra of the Au L_3-edge for the different samples we are studying. Typical XANES spectra of the fcc gold structure show three-peak patterns within the first 40 eV above the edge. The first resonance at the edge is often known as the white line, arising from $2p_{3/2,1/2} \rightarrow 5d$ dipole transitions, the intensity of which is very strong for most

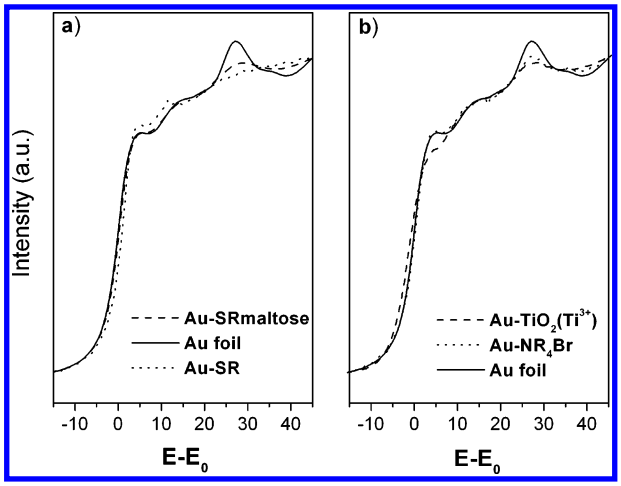

Figure 2. Au L_3-XANES spectra for different gold NPs compared to bulk gold (Au foil): (a) Au−SR and Au−SRmaltose samples and (b) Au−NR_4Br and Au−$TiO_2(Ti^{3+})$ samples.

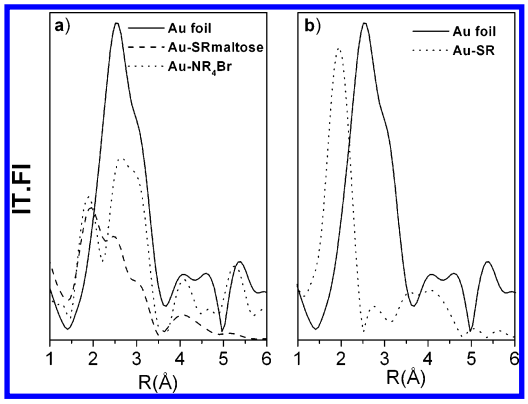

Figure 3. Modulus of the Fourier transform of EXAFS oscillations at the Au L_3-edge (*k* weighted; *k* space range of 3−12 Å without phase corrections) for the Au−SR, Au−SRmaltose, and Au−NR_4Br samples compared to bulk gold (Au foil).

transition metal with a partially filled d band and is related to the unoccupied density of d states (d-hole counts). Although the 5d orbitals in Au atoms are nominally full, due to s−p−d hybridation, a small white line can still be detected in the XANES of bulk Au.[17,18] The area under the white line can thus be used to study the d-charge redistributions in various gold samples.[17] In previous papers[2,4] it has been shown that small gold nanoparticles (around 2 nm in diameter), without strong interaction between surface gold atoms and the capping molecule, show a slight decrease in the white line intensity that indicates a gain in 5d electron density, relative to the bulk sample. Stronger Au d−d interactions favor s−p−d rehybridation, increasing the d-electron count at the Au site in the NPs[3]. This nanosize effect is also demonstrated by the lattice contraction observed in small gold clusters.[11]

In Figure 2b, a decrease in the intensity and the integrated area of the first resonance of the Au L_3-edge of sample Au−$TiO_2(Ti^{3+})$ is shown. According to the data in Table 1, this sample has an average particle size of 2 nm. However, if we compare our results with those previously reported by Zhang and Sham[4] for particles of similar size, without strong interaction of the gold surface atoms and the capping molecule, this decrease is here much more important. In fact, in this case, metal−support interaction phenomena must be taken into consideration. In a previous paper,[13] this effect has been interpreted as a result of a negative charge injection into the metal particles, which is favored by the presence of reduced species (Ti^{3+}) under photon irradiation of the colloidal TiO_2 support material.[13] Although this sample was exhaustively studied in this previous paper, we included it here as a nice example of how the electronic structure of gold NPs can be tuned upon control of their surface environments.

The opposite effect has been proposed[4] to be present in thiol-functionalized gold NPs, where the strong Au−S interaction has resulted in a d-charge transfer from gold to sulfur atoms.[19] In our case, two sulfur-derivatized Au NPs are reported showing average particle sizes, according to TEM, of 1.4 and 1.8 nm (respectively for Au−SR and Au−SRmaltose samples; see Table 1). The sample Au−SRmaltose shows a threshold resonance at the Au L_3 absorption that is just below the one for bulk gold (Figure 2a). In this case with particles of 1.8 nm in diameter, the lattice contraction effect is almost totally compensated by the charge transfer to the capping molecules. This is in good agreement with Zhang results[4] for 2 nm thiol-functionalized nanoparticles where the white line is just above the one for gold foil.

For the Au−SR sample, with an average particle size of 1.4 nm, we found a noticeable increase in the intensity of the Au L_3-threshold resonance (Figure 2a) that pointed out an important d-charge transfer from gold to sulfur atoms in this sample. At this point a complete and comparative structural and chemical analysis of both Au−SR and Au−SRmaltose samples is needed.

In addition, the Au−NR_4Br sample shows an intensity for the white line at the Au L_3-threshold identical to the intensity showed for the Au foil. This is in agreement with the behavior expected for a weak interaction between protective molecules and Au surface atoms and for the bimodal distribution of nanoparticles centered at 1.5 and 5.0 nm obtained for this sample.

Figure 3a,b represents the radial distribution functions obtained by Fourier transformation (FT) of the EXAFS oscillations over the K-range of 3−12 $Å^{-1}$ (not corrected for the phase shift). For the Au−SR and Au−SRmaltose samples, the peak discernible at 1.8 Å is attributed to the scattering of photoelectrons from the S atoms located at the nearest distances from the absorber Au atom,[20] while for the Au−NR_4Br sample the first peak at 1.7 Å is attributed to the C nearest atoms. In all samples the second peak at around 2.5 Å (with a shoulder at 3.0 Å) is due to the scattering of the first Au atom neighbor, as can be compared with the Au foil. The first feature that is remarkable in the FT curves is the strong intensity of the peak corresponding to the Au−S coordination shell, especially in the Au−SR sample. This result is in agreement with the strong intensity of the white line at the Au L_3-edge found for this sample (see Figure 2a), where the d-charge transfer from gold to sulfur atoms is the main factor controlling the electronic structure. Another remarkable feature in the FT curves in Figure 3 is the very small intensity of the second peak (Au−Au bonds) for the Au−SR sample, together with its position, which is not centered at the 2.5 Å position found for the Au foil reference sample but shifted to 2.7 Å. In addition to that, a peak is also detected in this sample at 3.5 Å which is present neither in the gold foil nor in the Au−SRmaltose sample.

With the aim to establish possible microstructural models for the thiol-capped gold NPs and to account for the EXAFS oscillations features, some calculations have been carried out. Several structural models have been built and their corresponding atom coordinates have been used as input for the FEFF6 program.[14] For each simulation, the result was achieved after averaging the sum of all EXAFS oscillations coming out by considering as absorption center every gold atom that constitute

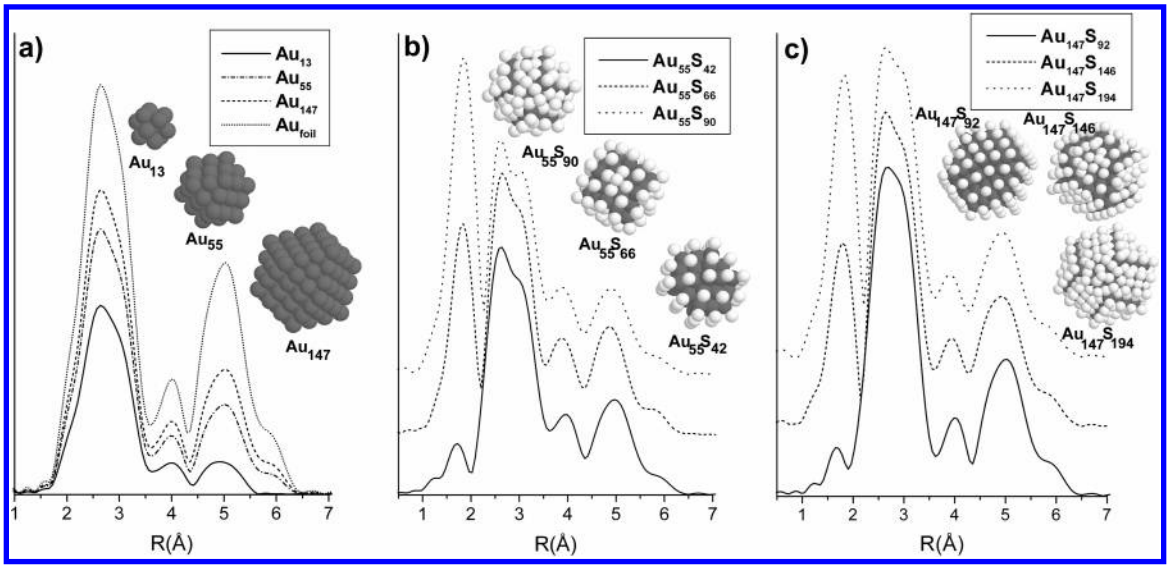

Figure 4. Clusters model simulations and FEFF6 calculated modulus of FT for EXAFS oscillations: (a) pure Au clusters, (b) Au_{55} clusters with increasing amounts of S atoms bound to surface gold atoms, and (c) Au_{147} clusters with increasing amounts of S atoms bound to surface gold atoms.

the model. In Figure 4, some of the modeled nanoparticles used to run the simulations as well as their calculated Fourier tranforms of EXAFS oscillations in the k-range of 3−12 $Å^{-1}$ are shown. Pure gold nanoparticles of 13, 55, and 147 atoms were used as references, which correspond to sizes of 0.8, 1.4, and 1.8 nm in diameter, respectively (see Figure 4a). The influence of adding new species linked onto the surface metal atoms was monitored by introducing in the original models sulfur atoms in specific positions with different surface symmetries (see Figure 4b,c).

As presented in Figure 4a for surface free gold nanoparticles, the Fourier transforms show a mean peak centered at 2.6 Å with a shoulder at ca. 3.0 Å that correspond to the Au−Au first coordination shell. As sulfur atoms are added to the surface of the particles, a new peak appears at around 1.8 Å, which accounts for the scattering process of photoelectrons from this light element located at the nearest distances (2.3 Å) from the absorber gold atom.[11] As revealed by the different calculations (Figure 4b,c), the relative intensity of this latter peak increases with respect to the Au−Au peaks with the increment of the number of sulfur atoms located on the surface. Furthermore, the intensity is closely dependent on the type of arrangement of these atoms, which could considerably change the coordination of the surface gold atoms. In all cases the sulfur atoms on the surface are located in such a way that every light atom coordinates only one metal atom, leading to very small intensities for the first peak observed in the Fourier transforms (see models $Au_{55}S_{42}$ and $Au_{147}S_{92}$ in Figure 4b,c). This result suggests that for reproducing the experimental FT curves described above (Figure 3), more than one sulfur atom per surface gold atom has to be considered. In the calculations, a high increment of the intensity of the first peak corresponding to Au−S bonds has been achieved by introducing extra sulfur atoms in positions that coordinate at the same time more than one surface gold atom. In this sense a high density of capping molecules is needed to obtain comparable intensities for the first peaks (Au−S and Au−Au) in the FT. With this theoretical analysis a possible qualitative explanation could be given for the features observed in the FT of EXAFS oscillations for Au−SRmaltose sample. A structure constituted by a core of fcc gold with a size between 1.4 and 1.8 nm and a protective layer constituted by more than one sulfur atom per surface gold atom could be a reasonable model.

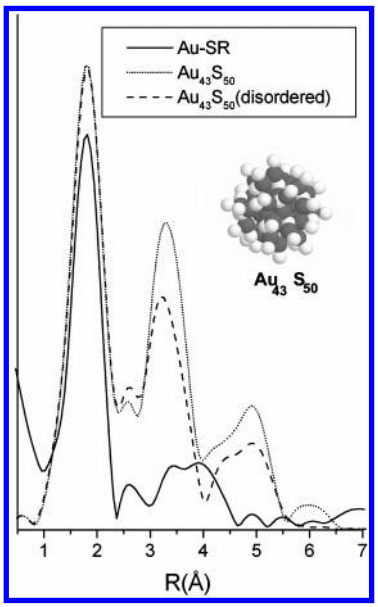

Figure 5. Cluster model simulation and FEFF6 calculated modulus of FT for EXAFS oscillations. Cluster model $Au_{43}S_{50}$ (13 atoms Au-core, AuS_2 shell, and S atoms bound to surface Au atoms). The experimental curve for the Au−SR sample has been included for comparison purposes.

In the case of the Au−SR sample, the FT obtained from its EXAFS oscillations (Figure 3b), in particular the very high relative intensity of the Au−S peak, the low intensity of the second peak (Au−Au), and its position at 2.8 Å as well as the appearance of a peak centered at 3.5 Å, is not reproduced by any of the simulations shown in Figure 4. To explain such a behavior, some extra simulations have been carried out considering more complex structures. A core−shell model has been proposed for the particles forming the Au−SR sample. In Figure 5, a particle constituted by a nucleus of 13 gold atoms with fcc structure and a shell with Au_2S structure is shown. An extra layer of sulfur atoms coordinating the surface metal atoms at a distance of 2.3 Å has also been considered in the model previous to running the simulations (see cluster model in Figure 5). The FT from the calculated EXAFS spectra reproduces quite well the main characteristics of the experimental results in Figure 3b. Note that in Figure 5 the first peak at around 1.8 Å increases its intensity at the expense of the second one centered now at

TABLE 2: Best Fitting Parameters of the Au L_3-edge EXAFS Oscillations for the Different Gold NPs

sample	atoms[a]	N[b]	R^c (Å)	σ^d (Å)	$\Delta\sigma^2 \times 10^{-3}$ (Å^2)	$\Delta E_0{}^e$ (eV)
Au foil	$(Au-Au)_m$	12	2.834	0.083		
Au−SRmaltose	(Au−S)	0.75	2.295	0.043	3.9	0.5
	$(Au-Au)_m$	5	2.778	0.104		
Au−SR	(Au−S)	1.3	2.297	0.042	5.2	−1.4
	$(Au-Au)_m$	2	2.984	0.125		
Au−NR_4Br	(Au−C)	1.9	2.204	0.049	0.5	−0.3
	$(Au-Au)_m$	8	2.837	0.086		

[a] Type of atoms in the coordination shell. [b] *N*: coordination number. [c] *R*: bond length. [d] σ: Debye−Waller factors. [e] Shift in the Au L_3 absorption edge.

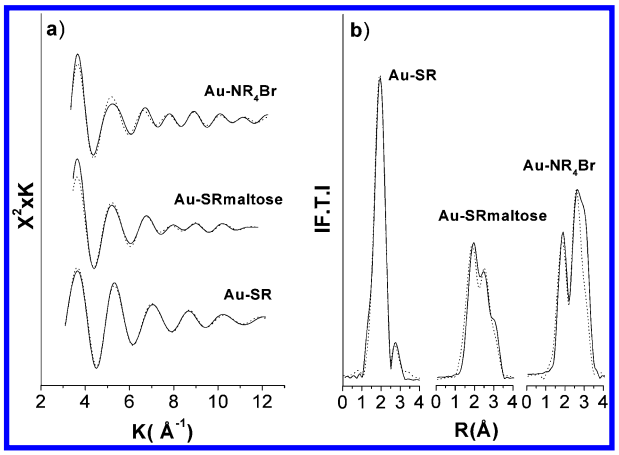

Figure 6. Experimental (−) and fitted (▪▪▪) EXAFS oscillations a) and radial distribution functions b) for Au−SR, Au−SRmaltose, and Au−NR_4Br samples. Fitting parameters are summarized in Table 2.

2.7 Å due to the diminishing number of Au−Au distances only present in the core of the particle. It is important to note at this point how the third peak at approximately 3.5 Å, arising from the Au−Au distances within the Au_2S shell structure, could account for the corresponding experimental signal. However, the intensity of such as peak is lower in the case of experimental data if compared with the calculation. It is also important to mention here that according to previous papers,[21] additional disorder may be considered in thiol-capped gold nanoparticles. This disorder has not been introduced in the original cluster models followed by FEFF6 simulations. This additional disorder may account for a more accurate matching between the experimental EXAFS oscillations and the simulated curves. The influence of such an effect on the calculated EXAFS signals is also exemplified in Figure 5. Some disorder has been introduced in the $Au_{43}S_{50}$ model in the sense of random displacements of gold atoms from their original coordinates. The magnitude of these movements was not bigger than 0.1 Å for each atom. The diminishing of intensities corresponding to the third and further coordination shells is clearly seen in the Fourier transform, resembling to some extend the features observed for the experimental data (Figure 3b).

Finally, the Fourier transform spectra for the three different capped systems were fitted by considering the contribution from the first (Au−S or Au−C) and second (Au−Au) shells to determine the following structural parameters: coordination numbers (*N*), bond distances (*r*), Debye Waller factors (σ), and the difference in the threshold energy from the bulk gold reference (see Table 2). Figure 6 shows fitted and experimental EXAFS oscillations and Fourier transforms for all the samples.

For the Au−SRmaltose sample, Au−Au and Au−S coordination numbers of 5.0 and 0.75 have been obtained, respectively. According to our cluster calculations for gold nanoparticles with an average particle diameter of 1.8 nm, ca. 63% of the total number of Au atoms are located at the surface (see Table 1). The Au−S coordination number of 0.75 is in agreement with a microstructure constituted by more than one thiol-alkyl chain bounded to each surface gold atom. The Au−Au bond length has been found to be 2.78 Å for the Au−SRmaltose sample, indicating a lattice contraction effect in comparison to the 2.83 Å parameter evaluated from the EXAFS analysis of the gold foil. These results are also in full agreement with the measured intensity of the white line at the Au L_3 threshold, where lattice contraction effects are compensated by Au−S charge-transfer effects, which result in a d-band electron density for the Au−SRmaltose sample similar to the one for bulk gold.

For the Au−SR sample, Au−Au and Au−S coordination numbers of 2.0 and 1.3 were found, respectively. According to clusters calculation for 1.4 nm size gold particles (see Table I), around 76% of the Au atoms may be located at the surface. The strong increase in the Au−S coordination number in comparison to the expected value of 0.76 can be explained if we consider a multiple Au−S bond. However, the strong decrease in the Au−Au coordination number indicates that not only surface gold atoms are affected by bonds to sulfur but also a Au_2S shell must be taken into consideration, as we also proposed in our model simulations. In this sample, Au−S charge-transfer effects are controlling the electronic structure of the gold clusters, leading to a strong white line intensity at the Au L_3-threshold. In addition to that, a Au−Au bond length of 2.98 Å has been estimated for this sample from EXAFS fitting analysis, which is a higher value that the one evaluated for the gold foil (2.83 Å). Charge transfer to the capping molecule is overcoming nanosize effects and also producing lattice expansion of the small Au−Au core cluster in this sample.

For the Au−NR_4Br sample, the capping molecule is a tetraoctylammonium salt, a weakly interacting dipole. Au−C and Au−Au coordination numbers of 1.9 and 8.0 have been obtained, respectively. The values are congruent with the higher average particle diameter of this sample, in which some particles have diameters in the range of 5 nm.

It is worth mentioning here that the semiquantitative EDX analysis of the samples gives a S:Au atomic ratio of ca. 1.0 and 0.6, respectively, for samples Au−SR and Au−SRmaltose (Table 1). This indicates, in agreement with the previously described EXAFS data that the Au−SR sample, prepared with excess of thiol-derivatized molecules, contains smaller gold nanoparticles strongly modified by Au−S bonds, in comparison to Au−SRmaltose. A quantitative agreement of model simulations with experimental EXAFS and chemical analysis data was not possible to achieve, because we did not have an adequate Au_2S reference compound and, more importantly, because thiol groups are introducing a strong distortion in the gold cluster core from the fcc order.[21] The polydispersity of nanoparticles, together with the many parameters involved during Fourier transform fitting, introduces additional limitations to the quantitative EXAFS analysis.

The EXAFS fitting analysis also shows that there is a shift in the gold L_3 absorption edge for the different capping systems. The ΔE_0 values summarized in Table 2 represent in a quantitative way this shift in the absorption threshold that can also be observed in the XANES spectra represented in Figure 2. The sample Au−SR showed the highest shift to higher threshold values as corresponds to a higher d-hole density at the gold atoms in comparison to the Au−SRmaltose sample. The higher

d-hole density is giving a higher binding energy for the electrons in the gold core levels.

The above-described XAS analysis clearly demonstrates how the nature of the capping system, as well as the microstructure, controls the electron/hole density at the d band, modifying the electronic behavior of gold nanoparticles. The magnetic properties obviously also depend on the same parameters that control the electronic behavior. The exhaustive microstructural analysis presented here is also relevant to understand the apparition of permanent magnetism, anisotropy, and hysteresis in thiol-capped gold NPs,[9] due to charge transfer effects together with the strong anisotropy of gold atoms submitted simultaneously to Au−Au and Au−S bonds.

Conclusions

Gold NPs have been prepared with different capping systems, and the XAS spectra (XANES and EXAFS regions) have been analyzed in detail. The weak interacting dipole molecules of the type tetralkylammonium salts produce a situation similar to naked gold NPs, where nanosize effects result in d−d interaction with a slightly increase in d charge at the Au site relative to the bulk for very small particles (bellow 2 nm in diameter). In the case of supported gold NPs on reduced TiO_2 porous phases, a strong increase in d electron density was observed at the NPs in comparison to bulk gold. This effect is due to charge transfer from reduced Ti^{3+} species in the TiO_2 phase. Contrary to the case of thiol-capped NPs, the charge transfer from the d states at the Au atoms to sulfur atoms bonded to gold is producing an increase in the d-hole density at the Au site that overcomes the d−d interaction due to pure size effects, provided that the nanoparticles are very small and the S:Au ratio is high enough.

The role of the EXAFS analysis was also very relevant, because it allowed us to determine the microstructure that produces the higher d-hole density in thiol-functionalized gold NPs. This microstructure, formed by a very small Au cluster surrounded by a shell formed by gold atoms bonded to sulfur, is also leading to a very singular magnetic behavior[9] of permanent magnetism and hysteresis, even at room temperature. The apparition of a strong distortion in the gold cluster core from the fcc order and the lack of an atomically abrupt Au−S interface were also pointed out during EXAFS analysis.

Acknowledgment. XAS facilities at BM29 in ESRF and the technical support from O. Mathon are acknowledged. The authors thank I. Rosa for technical assistance in sample preparation. Financial support from the Spanish MCyT, "Junta de Andalucía" and postdoctoral I3P program (CSIC) is also acknowledged.

References and Notes

(1) Alivisatos, A. P. *J. Phys. Chem.* **1996**, *100*, 13226.

(2) Coulthard, I.; Degen, I. S.; Zhu, Y.; Sham, T. K. *Can. J. Chem.* **1998**, *76*, 1707.

(3) Benfield, R.; Grandjean, D.; Kroll, M.; Pugin, R.; Sawitowski, T.; Schmid, G. *J. Phys. Chem.* **2001**, *105*, 1961.

(4) Zhang, P.; Sham, T. K. *Appl. Phys. Lett.* **2002**, *81*, 736.

(5) Cini, M.; Crescenzi, M.; Patella, F.; Motta, N.; Sastry, M.; Rocket, F.; Pasquali, R.; Balzarotti, A.; Verdozzi, C. *Phys. Rev. B* **1990**, *41*, 5685.

(6) Ohtani, K.; Fujikawa, T.; Kubota, T.; Asakura, K.; Iwasawa, Y. *Jpn. J. Appl. Phys. Part 1* **1998**, *37*, 4134.

(7) Tyson, C.; Bzowski, A.; Kristof, P.; Kuhn, M.; Sammynaiken, R.; Sham, T. K. *Phys. Rev. B* **1992**, *45*, 8924.

(8) Coulthard, I.; Sham, T. K. *Phys. Rev. Lett.* **1996**, *77*, 4824.

(9) Crespo, P.; Litrán, R.; Rojas, T. C.; Multigner, M.; de la Fuente, J. M.; Sánchez-López, J. C.; García, M. A.; Hernando, A.; Penadés, S.; Fernández, A. *Phys. Rev. Lett.* **2004**, *93*, 087204.

(10) Brust, M.; Walker, M.; Bethell, D.; Schiffrin, D. J.; Whyman, R. *J. Chem. Soc., Chem. Commun.* **1994**, 801.

(11) Zanchet, D.; Tolentino, H.; Martins Alves, M. C.; Alves, O. L.; Ugarte, D. *Chem Phys. Lett.* **2000**, *323*, 167.

(12) Barrientos, A. G.; de la Fuente, J. M.; Rojas, T. C.; Fernández, A.; Penadés, S. *Chem. Eur. J.* **2003**, *9*, 1909.

(13) Fernández, A.; Caballero, A.; González-Elipe, A. R.; Herrmann, J. M.; Dexpert, H.; Villain, F. *J. Phys. Chem.* **1995**, *99*, 3303.

(14) Zabinsky, S. I.; Rehr, J. J.; Ankudinov, A.; Albers, R. C.; Eller, M. J. *Phys. Rev. B* **1995**, *52*, 2995.

(15) Bernal, S.; Botana, F. J.; Calvino, J. J.; López-Cartes, C.; Pérez-Omil, J. A.; Rodríguez-Izquierdo, J. M. *Ultramiscroscopy* **1998**, *72*, 135.

(16) Bonin, D.; Kaiser, P.; Freitigny, C.; Desbarres, J. *Structures Fines d'e Absorption des Rayos X en Chimie, 3, Logiciels d'Analyse, EXAFS*; Dexpert, H., Michalowizc, A., Verdagner, M., Eds.; Societé Francaise de Chimie: Paris, 1989.

(17) Lytle, F. *Ber. Bunsen-Ges., Phys. Chem.* **1987**, *91*, 1251.

(18) Matheiss, L. R. *Dietz, Phys. Rev. B* **1980**, *22*, 1663.

(19) Hakkinen, H.; Barnett, R.; Landman, U. *Phys. Rev. Lett.* **1999**, *82*, 3264.

(20) Zhang, P.; Sham, T. K. *Phys. Rev. Lett.* **2003**, *90*, 245502.

(21) Garzón, I. L.; Rovira, C.; Michaelian, K.; Beltrán, M. R.; Ordejón, P.; Junquera, J.; Sánchez-Portal, D.; Artacho, E.; Soler, J. M. *Phys. Rev. Lett.* **2000**, *85*, 5250.